applied sciences

MDPI

Article

Tunable Degradation Rate and Favorable Bioactivity of Porous Calcium Sulfate Scaffolds by Introducing Nano-Hydroxyapatite

Jianhua Zhou [1,†], Fulai Yuan [2,†], Shuping Peng [3], Hui Xie [4], Ping Wu [5], Pei Feng [1], Chengde Gao [1], Youwen Yang [1,6], Wang Guo [1], Duan Lai [7], Zhiyang Zhou [7], Xueling Zhu [8] and Cijun Shuai [1,*]

1 State Key Laboratory of High Performance Complex Manufacturing, the State Key Laboratory for Powder Metallurgy, Central South University, Changsha 410083, China; zhouyx@csu.edu.cn (J.Z.); fengpei@csu.edu.cn (P.F.); gaochengde@csu.edu.cn (C.G.); yangyouwen@csu.edu.cn (Y.Y.); guowang@csu.edu.cn (W.G.)
2 Health Management Center, Xiangya Hospital, Central South University, Changsha 410008, China; fulaiyuan2010@163.com
3 The Key Laboratory of Carcinogenesis and Cancer Invasion of the Chinese Ministry of Education, the Key Laboratory of Carcinogenesis of the Chinese Ministry of Health and Cancer Research Institute, Xiangya Hospital, Central South University, Changsha 410078, China; shuping@csu.edu.cn
4 Motion System Injury Repair Research Center, Xiangya Hospital, Central South University, Changsha 410078, China; huixie@csu.edu.cn
5 College of Chemistry, Xiangtan University, Xiangtan 411105, China; pingwu@xtu.edu.cn
6 State Key Laboratory of Solidification Processing, Northwestern Polytechnical University, Xi'an 710072, China
7 Hunan Farsoon High-Technology Co. Ltd., Changsha 410205, China; laiduan@farsoon.com (D.L.); zhouzhiyang@farsoon.com (Z.Z.)
8 School of Humanities and Social Sciences, National University of Defense Technology, Changsha 410074, China; xuercan@163.com
* Correspondence: shuai@csu.edu.cn; Tel.: +86-731-8887-9351
† These authors contributed equally to this work.

Academic Editor: Daniel X.B. Chen
Received: 17 October 2016; Accepted: 30 November 2016; Published: 7 December 2016

Abstract: The bone scaffolds should possess suitable physicochemical properties and osteogenic activities. In this study, porous calcium sulfate ($CaSO_4$) scaffolds were fabricated successfully via selected laser sintering (SLS). Nano-hydroxyapatite (nHAp), a bioactive material with a low degradation rate, was introduced into $CaSO_4$ scaffolds to overcome the overquick absorption. The results demonstrated that nHAp could not only control the degradation rate of scaffolds by adjusting their content, but also improve the pH environment by alleviating the acidification progress during the degradation of $CaSO_4$ scaffolds. Moreover, the improved scaffolds were covered completely with the apatite spherulites in simulated body fluid (SBF), showing their favorable bioactivity. In addition, the compression strength and fracture toughness were distinctly enhanced, which could be ascribed to large specific area of nHAp and the corresponding stress transfer.

Keywords: selected laser sintering; porous scaffolds; degradation rate; pH environment; bioactivity

1. Introduction

Biodegradable scaffolds are becoming extremely promising objects for bone substitution and repair [1–4]. They can provide a temporary structural support for cell growth and migration, and act as an extracellular matrix to induce tissue regeneration [5,6]. Calcium sulfate ($CaSO_4$) is one of the most absorbable materials among all bioceramics. It possesses good biocompatibility and

osteoconduction [7,8]. However, $CaSO_4$ degrades too fast and decreases pH of the surrounding environment by releasing acidic products, resulting in an inflammatory reaction. In addition, $CaSO_4$ has poor bioactivity which cannot form an effective bone bond with the surrounding tissue [9,10].

Hydroxyapatite (HAp, $Ca_{10}(PO_4)_6(OH)_2$) is a necessary component of the bone tissue. It possesses numerous favorable properties like bioactivity, osteoinductivity, and nontoxicity [11,12]. Besides, HAp has slow biodegradability and presents alkalescency, which can neutralize the acidic product and maintain pH stabilization of the surrounding environment [13]. Moreover, nanoscale HAp is more efficient when used for bone repair compared with the conventional method, because it can stimulate tissue regeneration at the bone–implant interface [14]. Meanwhile, nano-hydroxyapatite (nHAp) possesses a large specific area, which can help to provide a strong interfacial interaction between nHAp and matrix, and thus enhance the mechanical strength [15].

In recent years, nHAp as a potential bioactive material and nano-reinforcing phase has been studied [16–18]. Sunil et al. added different contents of nHAp into magnesium and exhibited the ideal result of adjusting its degradation behavior and pH value during the immersion of samples in simulated body fluid (SBF) [19]. Covarrubias et al. investigated biological characteristics of nanoceramics and indicated that nHAp possessed the favorable ability to induce bone-like apatite formation, and promote protein adsorption and stem cell differentiation [20]. Chen et al. reported that nHAp was employed to intensify chitosan scaffolds by the biomimetic method, and showed that the mechanical strength and densification degree of scaffolds were not increased [21].

Selected laser sintering (SLS) is a novel processing technology in tissue engineering applications, which allows the sintering of powder materials in an exceedingly brief duration compared with the conventional sintering methods. Besides, it can easily construct a complex appearance and controllable porous structure of the scaffolds. Bone scaffolds formed using SLS possess an interconnected porous structure, which is beneficial for supporting cell adhesion, growth, and ingrowth of new bone tissue. In this study, nHAp was added to $CaSO_4$ and it was expected that tunable degradation rate and good bioactivity would be obtained. The $CaSO_4$/nHAp scaffold was prepared by SLS. The effects of nHAp on degradability, pH change trend, and bioactivity were tested by immersing the scaffold into the SBF solution. The mechanical property tests were carried out using the compression and indentation method. Furthermore, the biocompatibility was assessed by investigating the adhesion and proliferation behavior of the osteoblast-like cell on the scaffold.

2. Materials and Methods

2.1. Materials and Fabrication

Medical-grade $CaSO_4$ powder was obtained through Alfa Aesar China (Shanghai) Co., Ltd. (Shanghai, China) Parameters of the powder were as follows: purity: 99%, particle size: ~2 μm, density: 2.960 $g \cdot cm^{-3}$. The nHAp powder was bought from the Nanjing Emperor Nona Material Co., (Nanjing, China), and it was synthesized using $(CH_3O)_3$ and $Ca(NO_3)_2 \cdot 4H_2O$ as precursors by sol–gel method. The powder had a length of 150 nm and a diameter of 20 nm. Its purity and pH were 99.5% and 7.41, respectively. The $CaSO_4$ and nHAp powder in mass ratios of 95/5, 90/10, 85/15, and 80/20 were mixed, respectively. The mixed powder was dispersed into anhydrous alcohol and sonicated for two hours. Subsequently, the dispersed powder in suspension was filtered by filter paper and dried at 50 °C for six hours in an oven.

The mixed powder was used for preparing 3D porous scaffolds by a self-developed SLS system [22]. The whole system was made up of a control system, a motion platform, a support frame, and a focus system. The minimum laser spot was able to reach 100 μm by the laser focus system. The maximum laser power was 100 W. The process of laser sintering was as follows. Firstly, the mixed powder was paved onto the motion platform to obtain a thin powder layer. Then, a laser beam was conducted on a selected area of the powder to form a solid layer. Afterward, the motion

platform was lowered by an elevator to obtain the desired thickness of the monolayer. The above steps were constantly repeated layer-by-layer until the scaffold built. After removing unsintered powder, a scaffold with an interconnected porous structure was finally obtained. Preparation parameters of the scaffold are expressed in Table 1.

Table 1. Processing parameters of the scaffold.

Laser Power	Scanning Speed	Spot Diameter	Layer Thickness	Scan Spacing
7.5 W	100 mm·min^{-1}	1.0 mm	0.1 mm	3.5 mm

2.2. Characterization

The phase composition of the starting powder and the scaffold were detected by X-ray diffraction (XRD, Bruker-AXS, Karlsruhe, Germany). It was operated at 40 kV/250 mA and scanning speed of 8°/min with Cu Kα radiation. The results were recorded from 20° to 70° (step size: 0.1°/s). Distribution conditions of nHAp in the $CaSO_4$ matrix was obtained using scanning electron microscopy (SEM, TESCAN, Brno, Czech Republic) with energy dispersive spectroscopy (EDS). The scaffolds were fractured and placed on aluminum stubs. Then, the cross-sections were coated with a 10 nm platinum (Pt) layer using a sputter coater (JFC-1600, JEOL Co., Tokyo, Japan) due to poor conductivity of the scaffolds.

Compression tests of the scaffolds were conducted using a mechanical testing instrument (WD-01, Zhuoji Instruments, Shanghai, China) with the 100 N loading cell at a crosshead speed of 0.5 mm/min. The compressive strength was assessed by the recorded maximum loading. The toughness measurement was evaluated using Vickers indentation technique (HXD-1000TM, Taiming Optical Instrument Co., Shanghai, China). Indentation was carried out on the polished scaffolds surface by a diamond indenter at a loading of 4.9 N (ramp loading of 0.49 N/s and a dwell time of 15 s at maximum loading). Equation (1), proposed by Charles and Evans. was utilized for counting the fracture toughness (K_{IC}, MPa·m$^{1/2}$) [23]:

$$K_{IC} = 0.0824(P/c^{1.5}) \quad (1)$$

where P and c indicate the indentation loading (N) and the radial crack length (m), respectively.

2.3. SBF Immersion

The degradability of scaffolds was evaluated through the SBF soaking test. The SBF was prepared using the Kokubo method [24]. Inorganic aqueous solution (pH = 7.4) with ion concentration near human blood plasma was used [25]. Scaffolds with different contents of nHAp were soaked in SBF and kept at 37 °C. The ratio of scaffold surface area to SBF volume was kept at 1 cm^2 to 10 mL. The SBF was refreshed every two days. After finishing each immersion period, the scaffolds were taken away from solution and dried for 12 h at 60 °C.

The weight of scaffolds was measured before (W_0) and after soaking (W_t) to determine their degradation degree. The degradation (weight loss) was calculated using the following equation: Degradation = $(W_0 - W_t)/W_0 \times 100\%$. Meanwhile, the pH of soaking solution was measured every other day through an electrolyte-type pH meter (PHS-2C, Jingke Leici, Shanghai, China). Moreover, the apatite formation on the scaffolds was detected by SEM, EDS, and Fourier-transform infrared (FTIR, Thermo Scientific Co., Madison, WI, USA) technology.

2.4. Cell Culture

The osteosarcoma cell line (MG-63), purchased from the Cell Culture Center, (CCC, Chinese Academy of Medical Science, Beijing, China), was used for the test. The cells were revived by culturing into Dulbecco's Modified Eagle Medium (DMEM) with 10% (v/v) fetal bovine serum (FBS) at

37 °C in a humidified atmosphere. Then, cells were detached from cell culture plates using 0.03% ethylenediaminetetraacetic acid/0.25% trypsin solution. All scaffolds were sterilized by exposure to ultraviolet light for two hours. Afterwards, the cells were seeded dropwise onto the wetted scaffolds (5×10^3 cells/cm^2), and incubated at 37 °C for 1 day and 3 days. After incubation, the scaffolds with cells were fixed using glutaraldehyde, rinsed using phosphate-buffered saline (PBS), and dehydrated using various concentration of ethanol solution (20%–100%). Finally, the scaffolds were coated with Pt in vacuum and observed by SEM.

Calcein acetoxymethyl ester (AM) is a common fluorescent stain used for staining live cells. Before staining, the scaffolds with cells were fixed using 4% paraformaldehyde solution for 30 min and permeabilized using PBS with 0.5% Triton for 10 min. Then, the scaffolds were immersed with FBS, rinsed with PBS, stained with calcein AM, and placed in the dark for 5 min. After that, the scaffolds were rinsed using PBS and observed under fluorescent microscope (BX51, Olympus, Tokyo, Japan). In addition, cell proliferation behaviors were evaluated by the methylthiazol tetrazolium (MTT) assay. Firstly, the cells were cultivated on scaffolds for 1, 2, and 3 days, respectively. Then, 40 μL MTT solution (0.5 mg·mL^{-1}) was taken into cell culture plates and kept for 4 h at 37 °C. Dimethyl sulfoxide (DMSO) (200 mL) was added into the culture plate for completely dissolving the formazan product after medium was removed. In the end, 100 mL solution was removed and transferred to the new well plate. The absorbance was tested at 490 nm using the plate reader (VersaMaxTM, Molecular Devices, Sunnyvale, CA, USA).

2.5. Statistical Analysis

At least eight specimens were tested per group for the SBF immersion and mechanical property experiments, and five parallel specimens per group for the cell culture. The experimental data were analyzed using OriginPro 8.0 and reported as the mean + standard deviation. $p < 0.05$ (significance level) was considered statistically different.

3. Results and Discussion

3.1. Scaffolds Fabrication

The cylindrical scaffold was fabricated using SLS and is displayed in Figure 1, which had well-controlled open pores. The size of the scaffold was about 17.0 mm × 6.0 mm (diameter × height). The pores size and wall thickness were 1.5 mm and 2.0 mm, respectively. The pore channels were completely interconnected and distributed throughout the whole scaffold, which were necessary for new tissue ingrowth and vascularization construct [26]. Porosity of the cylindrical scaffold can be estimated as 30.8% by Equation (2) [27]:

$$P = (V_a - V_t)/V_a \quad (2)$$

where the porosity was designated as P (%), apparent volume was designated as V_a (mm^3), and true volume was designated as V_t (mm^3).

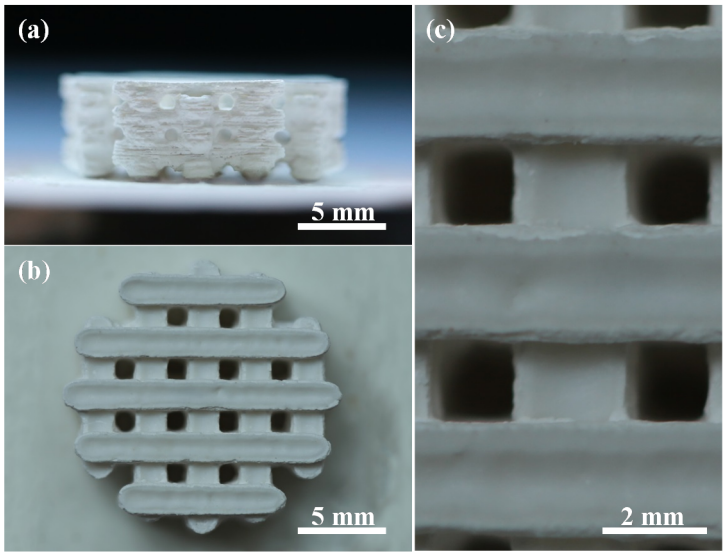

Figure 1. (**a**) Front view; (**b**) top view; and (**c**) enlarged view of the calcium sulfate/nano-hydroxyapatite ($CaSO_4$/nHAp) scaffold.

3.2. Phase and Microstructures

The phase composition of starting nHAp powder and the $CaSO_4$ scaffolds with different contents of nHAp was analyzed by XRD (Figure 2). It could be found in the patterns that the scaffolds were composed of HAp and $CaSO_4$ crystalline phase by comparison with the standard XRD pattern of HAp (JCPDS 72-1243) and $CaSO_4$ (JCPDS 70-0909). There were no other phases generated during the sintering process, which was in accordance with previous results of another researcher [28]. It was demonstrated that nHAp remained stable in the matrix, which could be compatible with $CaSO_4$.

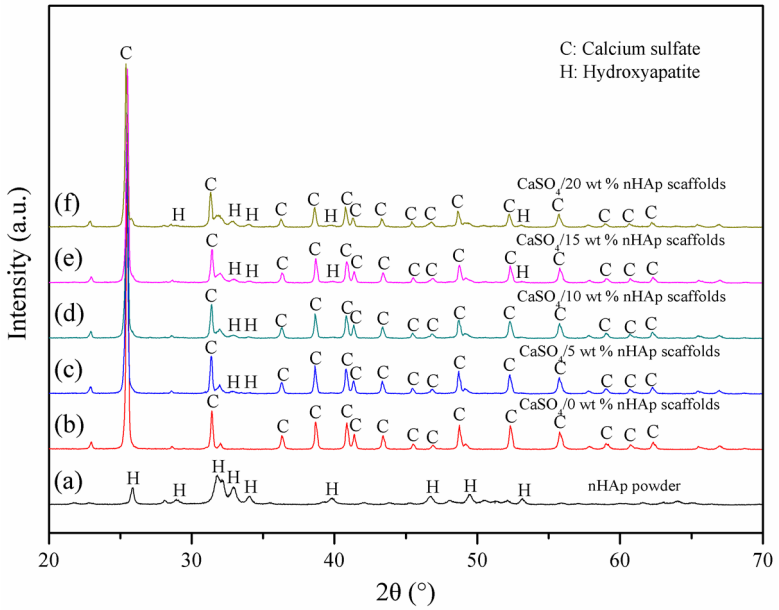

Figure 2. X-ray diffraction (XRD) patterns of (**a**) starting nHAp powder and the scaffolds with different contents of nHAp: (**b**) 0 wt %; (**c**) 5 wt %; (**d**) 10 wt %; (**e**) 15 wt %; and (**f**) 20 wt %.

In order to analyze the nHAp distribution in the $CaSO_4$ matrix, morphologies of the scaffolds at high magnifications were obtained by SEM (Figure 3). HAp nanoparticles were distributed as

primary particles in the microstructure of scaffolds containing 5, 10, and 15 wt % nHAp (Figure 3b–d). The particle size of some randomly selected HAp nanoparticles in these scaffolds was all in conformity with the particle size of starting nHAp powder. As the nHAp further increased to 20 wt %, agglomerates of the nanoparticles were observed (Figure 3e). Zamanian et al. also obtained similar distribution regularity of nanoparticles in the microstructure by adding nHAp into calcium hydroxide [29]. Fine ceramic particles tend to incorporate together under adhesion forces between particles, such as van der Waals forces or electrostatic forces.

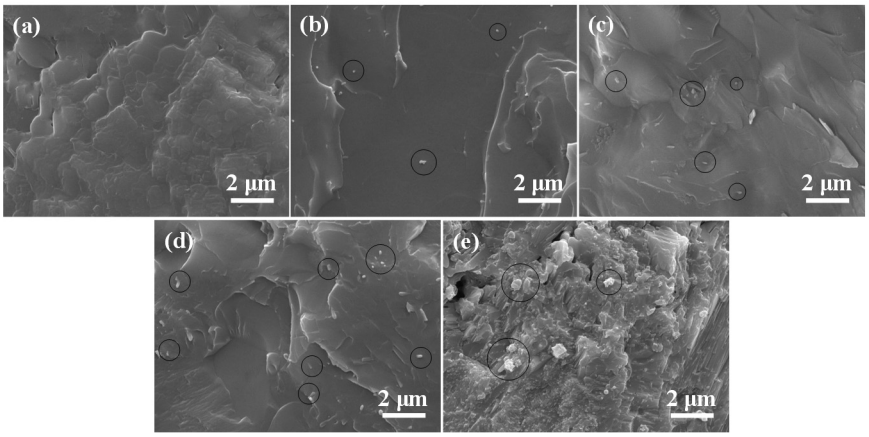

Figure 3. Cross-section of the scaffolds containing (**a**) 0 wt %; (**b**) 5 wt %; (**c**) 10 wt %; (**d**) 15 wt %; and (**e**) 20 wt % nHAp. The nanoparticles in circles indicate nHAp.

3.3. Degradability and pH

The $CaSO_4$ scaffolds containing various contents of nHAp were soaked in SBF solution for different periods to evaluate its degradability (Figure 4). It was found that the scaffolds without nHAp were nearly completely degraded within 21 days. Fast degradability of $CaSO_4$ was also confirmed by Kuo et al. [30]. After adding the nHAp, the degradation was obviously delayed and slowed gradually with increasing nHAp. Therefore, controlling the nHAp content is an efficient way to adjust the degradation rate of the scaffolds. The degradation rate decrease could be attributed to the fact that nHAp possesses a quite low degradability. Meanwhile, nHAp adherence to $CaSO_4$ could effectively reduce the contact of the $CaSO_4$ with the immersion solution and thus decrease the degradation rate of scaffolds.

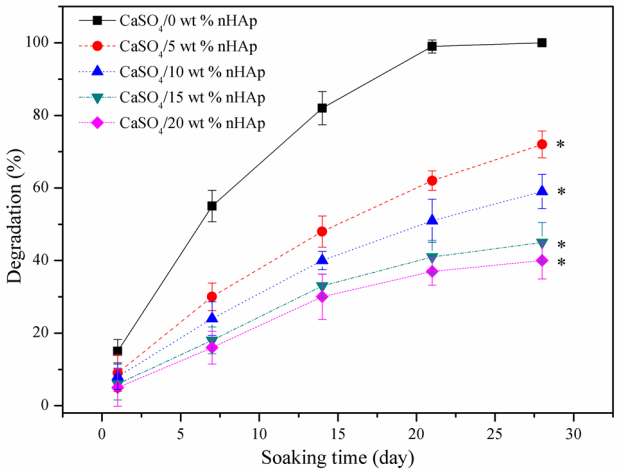

Figure 4. Degradation of the scaffolds after soaking in simulated body fluid (SBF) for different times. Significant difference between the composite scaffolds and pure $CaSO_4$ scaffolds (* $p < 0.05$).

The pH value changes of the SBF solution during the scaffolds immersion are shown in Figure 5. The solution presented an alkaline to acidic pH transition after soaking the scaffolds without nHAp, while the acidification progress of the immersion solution was alleviated effectively by introducing nHAp into the scaffolds. Moreover, the solution showed a mild alkaline pH (from 7.4 to 7.0) when nHAp contents increased to 15 or 20 wt %. This might be explained by nHAp presenting slight alkalinity, which was able to neutralize the acidic product of $CaSO_4$ and thus hinder the pH decrease. The improved pH environment could prevent inflammatory responses in vivo. In addition, it was reported that an alkaline environment was helpful for apatite formation and promoted its nucleation rate.

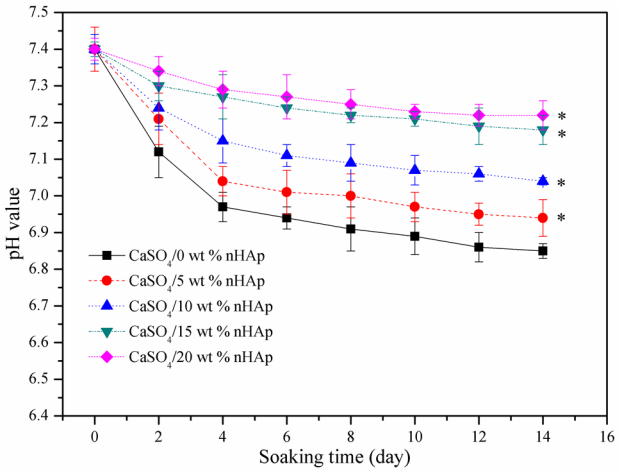

Figure 5. The pH value changes of SBF solution after the scaffolds soaking for different times. Significant difference between the composite scaffolds and pure $CaSO_4$ scaffolds (* $p < 0.05$).

3.4. Mechanical Property

The effect of nHAp on the mechanical property of the scaffolds is shown in Figure 6. The compressive strength was enhanced gradually with nHAp increasing from 0 to 15 wt %. Subsequently, the strength declined when the nHAp increased further to 20 wt %. Meanwhile, the fracture toughness exhibited a similar change trend and arrived to the peak value at 15 wt % nHAp content. Peak values of the strength and toughness were 34.46 MPa and 1.41 MPa·$m^{1/2}$, which increased by 68% and 29%, respectively, compared with that of the scaffolds without nHAp.

The mechanical property improvement was attributed to uniform dispersion of HAp nanoparticles and the corresponding stress transfer. HAp nanoparticles had the strong interfacial bonding with the $CaSO_4$ matrix due to its large specific area (50 m^2/g). Under the loading, the stress could be transferred between HAp nanoparticles and the matrix. The high-stress region would be released and transferred to another region, and thus enhance the loading resistance of scaffolds. On the other hand, excessive nHAp would form an agglomerate structure and reduce the bonding interface area between the matrix and nHAp, which would result in stress concentration and some inner flaws in the matrix, such as voids and cracks, weakening its mechanical strength [31].

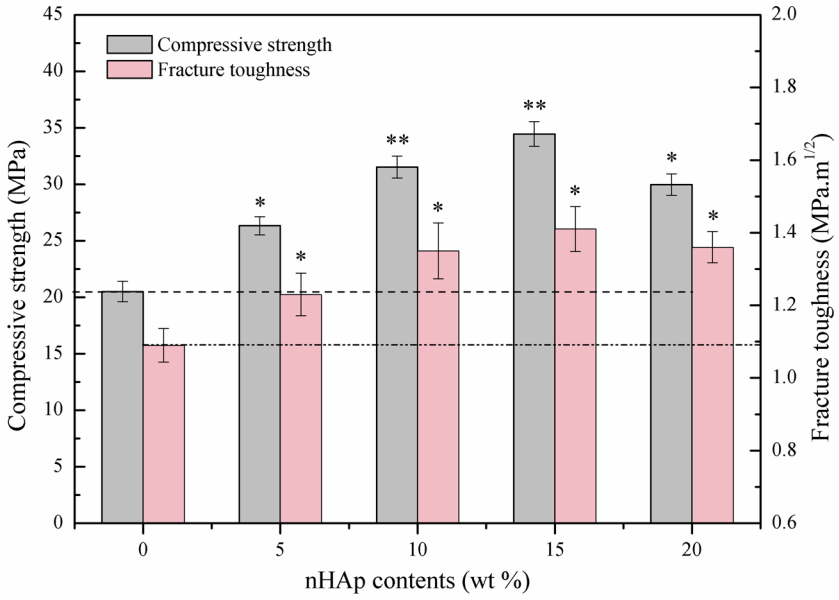

Figure 6. Compressive strength and fracture toughness of the scaffolds at different nHAp contents. Significant difference between the composite scaffolds and pure $CaSO_4$ scaffolds (* $p < 0.05$, ** $p < 0.01$).

3.5. Bioactivity

Bioactivity of the scaffolds was assessed by soaking in SBF for 1 and 3 days, respectively (Figure 7). The results demonstrated that there was a lot of spherical precipitate with bonelike apatite shape on the scaffolds containing nHAp. Besides, most of the scaffold's surface was covered by the apatite precipitate after soaking for 3 days when the nHAp increased to 15 wt %. The scaffolds containing 20 wt % nHAp was covered completely by the apatite precipitate at that time. The precipitate did not appear on the control group. As multiple studies have pointed out, there is no apatite formation on the pure $CaSO_4$ during soaking in SBF [32,33], which coincides with the experimental result in this test. The EDS analysis (Figure 8a) further demonstrated that the precipitate layer on the scaffolds was mainly composed of calcium (Ca) and phosphorus (P). Their ratio was about 1.74, which is close to the stoichiometric ratio of Ca/P in the apatite (1.67).

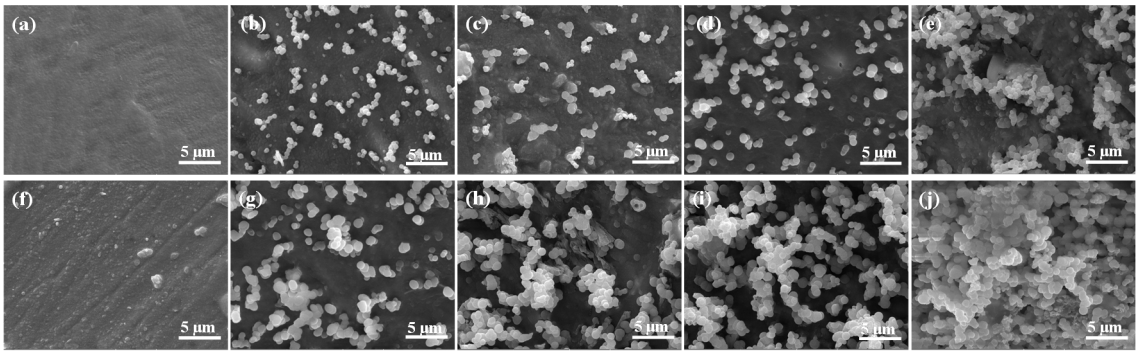

Figure 7. Morphologies of the scaffolds containing (**a**,**f**) 0 wt % (control); (**b**,**g**) 5 wt %; (**c**,**h**) 10 wt %; (**d**,**i**) 15 wt %; and (**e**,**j**) 20 wt % nHAp after soaking in SBF for (**a**–**e**) 1 day and (**f**–**j**) 3 days.

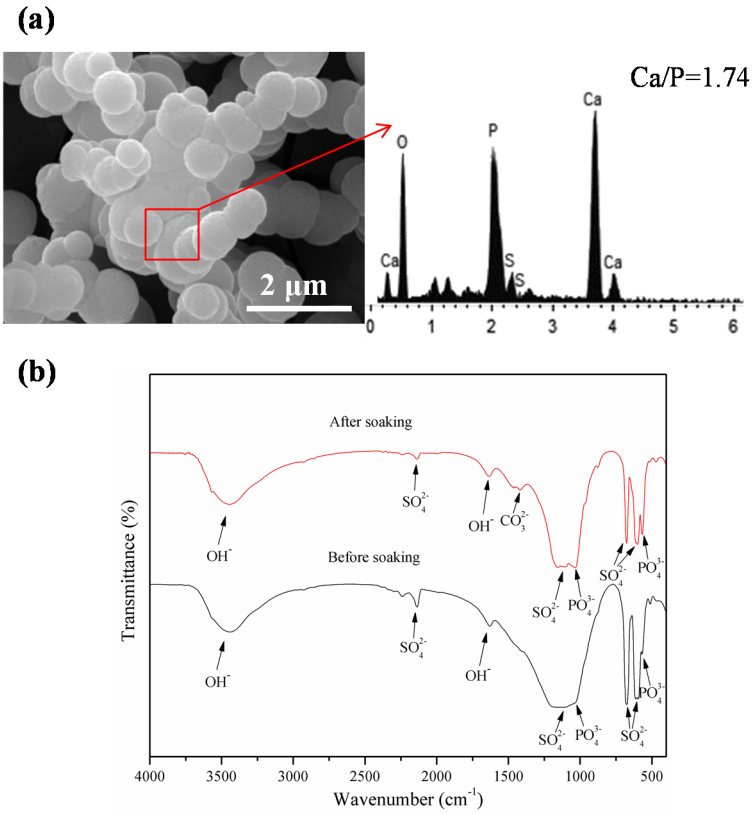

Figure 8. (**a**) Scanning electron microscopy (SEM) and energy dispersive spectroscopy (EDS) analysis of the precipitate on the $CaSO_4$/15 wt % nHAp scaffolds after soaking in SBF for 3 days; (**b**) Fourier-transform infrared (FTIR) spectra of the $CaSO_4$/15 wt % nHAp scaffolds soaked in SBF for 3 days.

In addition, composition of the scaffolds with 15 wt % nHAp before and after soaking was also analyzed by FTIR spectroscopy (Figure 8b). The intensity of PO_4^{3-} absorption bands, located at around 567 cm^{-1} and 1035 cm^{-1}, presented a significant increase. Moreover, the CO_3^{2-} absorption bands were observed at 1418 cm^{-1} in the scaffolds after soaking, which did not appear in the scaffolds before soaking. All of these results confirmed that the bonelike apatite formed on the scaffold after soaking.

The nHAp played an important role in the apatite formation, which was able to serve as the nucleation site for the apatite crystal growth in SBF. The apatite layer in the biological environment could greatly promote the formation of strong bone bonds between the scaffolds and bone tissues, as well as bone regeneration progress [34,35]. Besides, the apatite, covering the scaffolds, slowed the degradation rate of the scaffolds by reducing its contact with the soaking solution.

3.6. Cell Adhesion and Proliferation

The cell morphologies on the scaffolds were analyzed by SEM and fluorescent staining (Figures 9 and 10). In comparison to the rounded cells in the control group, the cells on the scaffolds with nHAp spread well after cultivating for 1 day and exhibited a fusiform morphology. Besides, the extension degree of the cells gradually enhanced with increasing nHAp content. After 3 days, the cells formed a confluent layer by cytoplasmic extension and attached closely throughout the scaffolds. The MTT assay was used for investigating the cell proliferation behavior after culturing for 1, 2, and 3 days, respectively (Figure 11). The experimental result showed that the cells presented a good proliferation trend on the scaffolds with the culture time extension. Meanwhile, the cells numbers on the scaffolds with nHAp was obviously higher than that of the control group.

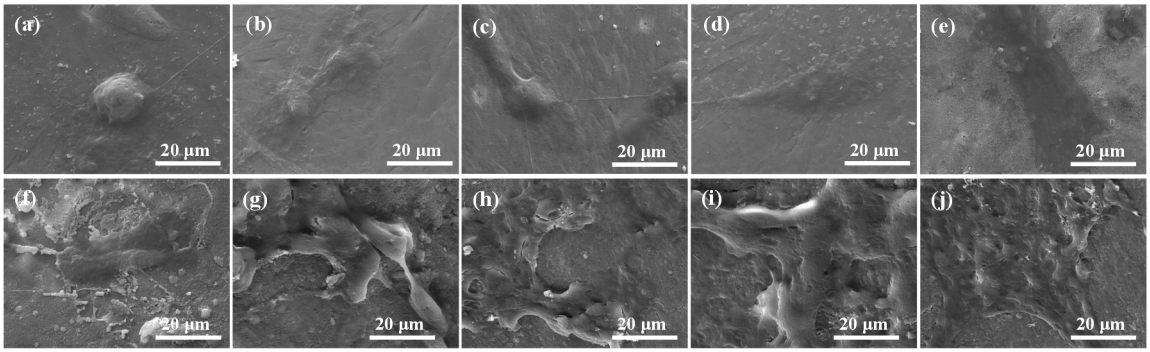

Figure 9. SEM images of MG-63 cells cultured on the scaffolds containing (**a**,**f**) 0 wt % (control); (**b**,**g**) 5 wt %; (**c**,**h**) 10 wt %; (**d**,**i**) 15 wt %; and (**e**,**j**) 20 wt % nHAp for (**a**–**e**) 1 day and (**f**–**j**) 3 days.

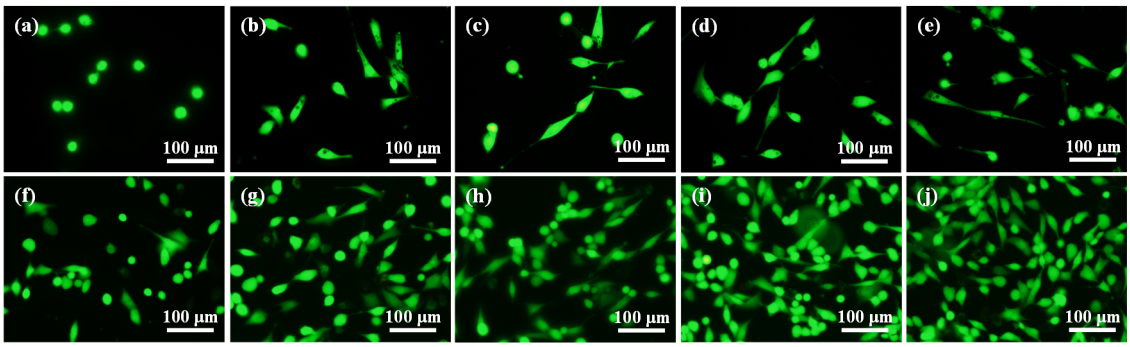

Figure 10. Fluorescent images of MG-63 cells cultured on the scaffolds containing (**a**,**f**) 0 wt % (control); (**b**,**g**) 5 wt %; (**c**,**h**) 10 wt %; (**d**,**i**) 15 wt %; and (**e**,**j**) 20 wt % nHAp for (**a**–**e**) 1 day and (**f**–**j**) 3 days.

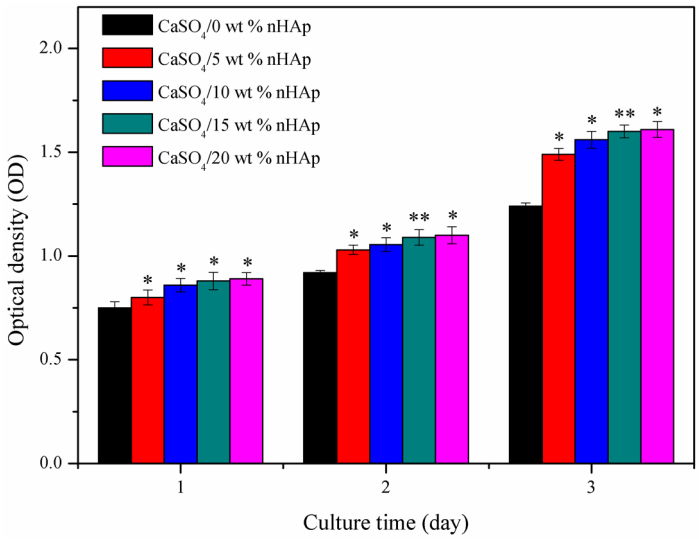

Figure 11. Proliferation behaviors of cells cultivated on the scaffolds for 1, 2, and 3 days. Significant difference between the composite scaffolds and pure $CaSO_4$ scaffolds (* $p < 0.05$, ** $p < 0.01$).

The results of cell culture suggested that the scaffolds containing nHAp could promote cell growth and proliferation, showing good biocompatibility. This was due to the fact that nHAp helps to adsorb more protein, such as fibronectin or vitronectin, on the scaffold's surface. The adsorbed protein attracts more cells towards this region and thus enhanced the cell adhesion and proliferation ability.

In addition, nHAp restrained the acidification effect during $CaSO_4$ degradation and created a slightly alkaline environment, which is beneficial for supporting cell metabolism.

4. Conclusions

In this study, nHAp was added to $CaSO_4$ to obtain the bioactive scaffolds with a tunable degradation rate, which was prepared through the SLS. The SBF immersion test showed that the nHAp was able to effectively improve degradability and apatite-formation ability of the scaffolds. Besides, the scaffolds containing nHAp showed a good ability to prevent decreasing pH during degradation; this is due to the neutralizing effect of nHAp on the acidic degradation byproducts released from $CaSO_4$. Moreover, the mechanical strength was correspondingly enhanced while increasing nHAp to 15 wt %, while further increasing nHAp led to decreased mechanical strength due to agglomeration of nanoparticles in the matrix. The cell culture experiment demonstrated that the composite scaffolds had excellent biocompatibility to support cell attachment and proliferation. Therefore, the $CaSO_4$/nHAp scaffold is a very promising candidate for bone defect treatment.

Acknowledgments: This work was supported by the following funds: (1) The Natural Science Foundation of China (51575537, 81572577); (2) Overseas, Hong Kong & Macao Scholars Collaborated Researching Fund of National Natural Science Foundation of China (81428018); (3) Hunan Provincial Natural Science Foundation of China (14JJ1006, 2016JJ1027); (4) The Project of Innovation-driven Plan of Central South University (2015CXS008, 2016CX023); (5) The Open-End Fund for the Valuable and Precision Instruments of Central South University; (6) The fund of the State Key Laboratory of Solidification Processing in NWPU (SKLSP201605); (7) The fund of the State Key Laboratory for Powder Metallurgy; (8) The Fundamental Research Funds for the Central Universities of Central South University.

Author Contributions: Jianhua Zhou and Fulai Yuan finished experiments designing and paper writing. Shuping Peng, Hui Xie and Ping Wu operated SBF and cell culture test. Pei Feng, Chengde Gao, Youwen Yang, Wang Guo operated mechanical property and ingredient test. Duan Lai, Zhiyang Zhou and Xueling Zhu involved in data analysis and results discussion. All experimental operation, data analysis and results discussion were conducted under the guidance of Cijun Shuai.

Conflicts of Interest: Authors declare no conflict of interest with respect to the authorship, research, and publication of this article.

References

1. Sheikh, Z.; Najeeb, S.; Khurshid, Z.; Verma, V.; Rashid, H.; Glogauer, M. Biodegradable materials for bone repair and tissue engineering applications. *Materials* **2015**, *8*, 5744–5794.
2. Martínez-Vázquez, F.J.; Cabanas, M.V.; Paris, J.L.; Lozano, D.; Vallet-Regí, M. Fabrication of novel Si-doped hydroxyapatite/gelatine scaffolds by rapid prototyping for drug delivery and bone regeneration. *Acta Biomater.* **2015**, *15*, 200–209. [CrossRef] [PubMed]
3. Lee, Y.C.; Chen, C.; Tsai, X.T. Visualizing the Knowledge Domain of Nanoparticle Drug Delivery Technologies: A Scientometric Review. *Appl. Sci.* **2016**, *6*, 11. [CrossRef]
4. Thuaksuban, N.; Luntheng, T.; Monmaturapoj, N. Physical characteristics and biocompatibility of the polycaprolactone–biphasic calcium phosphate scaffolds fabricated using the modified melt stretching and multilayer deposition. *J. Biomater. Appl.* **2016**, *30*, 1460–1472. [CrossRef] [PubMed]
5. Tong, S.; Xu, D.P.; Liu, Z.M.; Du, Y.; Wang, X.K. Synthesis of the New-Type Vascular Endothelial Growth Factor–Silk Fibroin–Chitosan Three-Dimensional Scaffolds for Bone Tissue Engineering and In Vitro Evaluation. *J. Craniofac. Surg.* **2016**, *27*, 509–515. [CrossRef] [PubMed]
6. Kim, M.S.; Lee, M.H.; Kwon, B.J.; Koo, M.A.; Seon, G.M.; Park, J.C. Enhancement of human mesenchymal stem cell infiltration into the electrospun poly(lactic-co-glycolic acid) scaffold by fluid shear stress. *Biochem. Biophys. Res. Commun.* **2015**, *463*, 137–142. [CrossRef] [PubMed]
7. Karr, J.C.; Lauretta, J. In vitro activity of calcium sulfate and hydroxyapatite antifungal disks loaded with amphotericin B or voriconazole in consideration for adjunctive osteomyelitis management. *J. Am. Podiatr. Med. Assoc.* **2015**, *105*, 104–110. [CrossRef]
8. Gu, J.; Wang, T.; Fan, G.; Ma, J.; Hu, W.; Cai, X. Biocompatibility of artificial bone based on vancomycin loaded mesoporous silica nanoparticles and calcium sulfate composites. *J. Mater. Sci. Mater. Med.* **2016**, *27*, 1–11. [CrossRef]

9. Chang, M.P.; Tsung, Y.C.; Hsu, H.C.; Tuan, W.H.; Lai, P.L. Addition of a small amount of glass to improve the degradation behavior of calcium sulfate bioceramic. *Ceram. Int.* **2015**, *41*, 1155–1162.
10. Shen, Y.; Yang, S.; Liu, J.; Xu, H.; Shi, Z.; Lin, Z.; Ying, X.Z.; Guo, P.; Lin, T.; Yan, S.G.; et al. Engineering scaffolds integrated with calcium sulfate and oyster shell for enhanced bone tissue regeneration. *ACS Appl. Mater. Interfaces* **2014**, *6*, 12177–12188. [CrossRef] [PubMed]
11. Shakir, M.; Jolly, R.; Khan, M.S.; Iram, N.E.; Sharma, T.K.; Al-Resayes, S.I. Synthesis and characterization of a nano-hydroxyapatite/chitosan/polyethylene glycol nanocomposite for bone tissue engineering. *Polym. Adv. Technol.* **2015**, *26*, 41–48. [CrossRef]
12. Chen, L.; Hu, J.; Ran, J.; Shen, X.; Tong, H. A novel nanocomposite for bone tissue engineering based on chitosan–silk sericin/hydroxyapatite: Biomimetic synthesis and its cytocompatibility. *RSC Adv.* **2015**, *5*, 56410–56422. [CrossRef]
13. Manchon, A.; Alkhraisat, M.; Rueda-Rodriguez, C.; Torres, J.; Prados-Frutos, J.C.; Ewald, A.; López-Cabarcos, E. Silicon calcium phosphate ceramic as novel biomaterial to simulate the bone regenerative properties of autologous bone. *J. Biomed. Mater. Res. Part A* **2015**, *103*, 479–488. [CrossRef] [PubMed]
14. Venkatesan, J.; Lowe, B.; Anil, S.; Kim, S.K.; Shim, M.S. Combination of Nano-Hydroxyapatite with Stem Cells for Bone Tissue Engineering. *J. Nanosci. Nanotechnol.* **2016**, *16*, 8881–8894. [CrossRef]
15. Shuai, C.; Feng, P.; Yang, B.; Cao, Y.; Min, A.; Peng, S. Effect of nano-zirconia on the mechanical and biological properties of calcium silicate scaffolds. *Int. J. Appl. Ceram. Technol.* **2015**, *12*, 1148–1156. [CrossRef]
16. Kailasanathan, C.; Selvakumar, N. Comparative study of hydroxyapatite/gelatin composites reinforced with bio-inert ceramic particles. *Ceram. Int.* **2012**, *38*, 3569–3582. [CrossRef]
17. Chan, K.W.; Wong, H.M.; Yeung, K.W.K.; Tjong, S.C. Polypropylene biocomposites with boron nitride and nanohydroxyapatite reinforcements. *Materials* **2015**, *8*, 992–1008. [CrossRef]
18. Cao, S.; Li, H.; Li, K.; Lu, J.; Zhang, L. In vitro mineralization of MC3T3-E1 osteoblast-like cells on collagen/nano-hydroxyapatite scaffolds coated carbon/carbon composites. *J. Biomed. Mater. Res. Part A* **2016**, *104*, 533–543. [CrossRef] [PubMed]
19. Sunil, B.R.; Kumar, T.S.S.; Chakkingal, U.; Nandakumar, V.; Doble, M. Friction stir processing of magnesium–nanohydroxyapatite composites with controlled in vitro degradation behavior. *Mater. Sci. Eng. C* **2014**, *39*, 315–324. [CrossRef] [PubMed]
20. Covarrubias, C.; Arroyo, F.; Balanda, C.; Neira, M.; Von Marttens, A.; Caviedes, P.; Rodríguez, J.P.; Urra, C. The effect of the nanoscale structure of nanobioceramics on their in vitro bioactivity and cell differentiation properties. *J. Nanomater.* **2015**, *2015*, 526230–526243. [CrossRef]
21. Chen, J.; Zhang, G.; Yang, S.; Li, J.; Jia, H.; Fang, Z.; Zhang, Q. Effects of in situ and physical mixing on mechanical and bioactive behaviors of nano hydroxyapatite–chitosan scaffolds. *J. Biomater. Sci. Polym. Ed.* **2011**, *22*, 2097–2106. [CrossRef] [PubMed]
22. Yang, Y.; Wu, P.; Lin, X.; Liu, Y.; Bian, H.; Zhou, Y.; Gao, C.; Shuai, C. System development, formability quality and microstructure evolution of selective laser-melted magnesium. *Virtual Phys. Prototyp.* **2016**, *11*, 173–181. [CrossRef]
23. Veljovíc, D.; Zalite, I.; Palcevskis, E.; Smiciklas, I.; Petrovíc, R.; Janáckovíc, D. Microwave sintering of fine grained HAP and HAP/TCP bioceramics. *Ceram. Int.* **2010**, *36*, 595–603. [CrossRef]
24. Lin, K.; Zhang, M.; Zhai, W.; Qu, H.; Chang, J. Fabrication and characterization of hydroxyapatite/wollastonite composite bioceramics with controllable properties for hard tissue repair. *J. Am. Ceram. Soc.* **2011**, *94*, 99–105. [CrossRef]
25. Wang, Y.; Yang, X.; Gu, Z.; Qin, H.; Li, L.; Liu, J.; Yu, X. In vitro study on the degradation of lithium-doped hydroxyapatite for bone tissue engineering scaffold. *Mater. Sci. Eng. C* **2016**, *66*, 185–192. [CrossRef] [PubMed]
26. Fedorovich, N.E.; Alblas, J.; Hennink, W.E.; Öner, F.C.; Dhert, W.J. Organ printing: The future of bone regeneration? *Trends Biotechnol.* **2011**, *29*, 601–606. [CrossRef] [PubMed]
27. Zein, I.; Hutmacher, D.W.; Tan, K.C.; Teoh, S.H. Fused deposition modeling of novel scaffold architectures for tissue engineering applications. *Biomaterials* **2002**, *23*, 1169–1185. [CrossRef]
28. Yang, D.; Yang, Z.; Li, X.; Di, L.Z.; Zhao, H. A study of hydroxyapatite/calcium sulphate bioceramics. *Ceram. Int.* **2005**, *31*, 1021–1023. [CrossRef]
29. Zamanian, A.; Yasaei, M.; Moztarzadeh, F.; Hesaraki, S.; Hafezi, M. Influence of nano-hydroxyapatite addition to calcium hydroxide cement on its Properties. *Key Eng. Mater.* **2012**, *493*, 655–660. [CrossRef]

30. Kuo, S.T.; Wu, H.W.; Tuan, W.H. Resorbable calcium sulfates with tunable degradation rate. *J. Asian Ceram. Soc.* **2013**, *1*, 102–107. [CrossRef]
31. Niu, L.N.; Fang, M.; Jiao, K.; Tang, L.H.; Xiao, Y.H.; Shen, L.J.; Chen, J.H. Tetrapod-like zinc oxide whisker enhancement of resin composite. *J. Dent. Res.* **2010**, *89*, 746–750. [CrossRef] [PubMed]
32. Chen, C.C.; Wang, C.W.; Hsueh, N.S.; Ding, S.J. Improvement of in vitro physicochemical properties and osteogenic activity of calcium sulfate cement for bone repair by dicalcium silicate. *J. Alloys Compd.* **2014**, *585*, 25–31. [CrossRef]
33. Cabanas, M.V.; Rodriguez-Lorenzo, L.M.; Vallet-Regi, M. Setting behavior and in vitro bioactivity of hydroxyapatite/calcium sulfate cements. *Chem. Mater.* **2002**, *14*, 3550–3555. [CrossRef]
34. Kalia, P.; Vizcay-Barrena, G.; Fan, J.P.; Warley, A.; Di Silvio, L.; Huang, J. Nanohydroxyapatite shape and its potential role in bone formation: an analytical study. *J. R. Soc. Interface* **2014**, *11*. [CrossRef] [PubMed]
35. Cabrejos-Azama, J.; Alkhraisat, M.H.; Rueda, C.; Torres, J.; Blanco, L.; López-Cabarcos, E. Magnesium substitution in brushite cements for enhanced bone tissue regeneration. *Mater. Sci. Eng. C* **2014**, *43*, 403–410. [CrossRef] [PubMed]